Research article

Jianyang Zhou, Feng Tao, Jinfeng Zhu*, Shaowei Lin, Zhengying Wang, Xiang Wang, Jun-Yu Ou, Yuan Li and Qing Huo Liu

Portable tumor biosensing of serum by plasmonic biochips in combination with nanoimprint and microfluidics

https://doi.org/10.1515/nanoph-2018-0173
Received October 12, 2018; revised December 18, 2018; accepted December 18, 2018

Abstract: Plasmonic sensing has a great potential in the portable detection of human tumor markers, among which the carcinoembryonic antigen (CEA) is one of the most widely used in clinical medicine. Traditional plasmonic and non-plasmonic methods for CEA biosensing are still not suitable for the fast developing era of Internet of things. In this study, we build up a cost-effective plasmonic immunochip platform for rapid portable detection of CEA by combining soft nanoimprint lithography, microfluidics, antibody functionalization, and mobile fiber spectrometry. The plasmonic gold nanocave array enables stable surface functionality, high sensitivity, and simple reflective measuring configuration in the visible range. The rapid quantitative CEA sensing is implemented by a label-free scheme, and the detection capability for the concentration of less than 5 ng/ml is achieved in clinical experiments, which is much lower than the CEA cancer diagnosis threshold of 20 ng/ml and absolutely sufficient for medical applications. Clinical tests of the chip on detecting human serums demonstrate good agreement with conventional medical examinations and great advantages on simultaneous multichannel detections for high-throughput and multi-marker biosensing. Our platform provides promising opportunities on low-cost and compact medical devices and systems with rapid and sensitive tumor detection for point-of-care diagnosis and mobile healthcare.

Keywords: plasmonics; nanoimprint lithography; biosensing; microfluidics; immunochip.

***Corresponding author: Jinfeng Zhu,** School of Electronic Science and Engineering, Xiamen University, Xiamen 361005, China, e-mail: nanoantenna@hotmail.com.
https://orcid.org/0000-0003-3666-6763
Jianyang Zhou, Feng Tao and Zhengying Wang: School of Electronic Science and Engineering, Xiamen University, Xiamen 361005, China
Shaowei Lin: The First Affiliated Hospital of Xiamen University, Xiamen 361003, China
Xiang Wang: State Key Laboratory of Physical Chemistry of Solid Surfaces, College of Chemistry and Chemical Engineering, Xiamen University, Xiamen 361005, China
Jun-Yu Ou: Optoelectronics Research Centre and Centre for Photonic Metamaterials, University of Southampton, Highfield, Southampton SO17 1BJ, UK
Yuan Li: Central Laboratory of Yongchuan Hospital, Chongqing Medical University, Yongchuan 402160, China
Qing Huo Liu: Department of Electrical and Computer Engineering, Duke University, Durham, NC 27708, USA

1 Introduction

Carcinoembryonic antigen (CEA) is one of the most widely used tumor markers in medicine and has been intensively studied in clinical analysis. Serum from individuals with gastrointestinal cancers often has higher levels of CEA than healthy individuals [1–3]. CEA levels may also be raised in pancreatic carcinoma, lung carcinoma, breast carcinoma and ovarian carcinoma [4–7]. CEA levels over 20 ng/ml are usually associated with patients having cancer in the metastatic state [8]. Therefore, the detection of CEA has great significance for the diagnosis and prognosis of cancer, especially at an early stage of the disease. Currently, chemiluminescence immunoassay (CLIA) and enzyme-linked immunosorbent immunoassay (ELISA) have been generally used for the detection of CEA in the clinical field. Both of them are laboratory-based techniques and inevitably suffer from some shortcomings, such as sample labeling, large volume, high expense, and complicated configurations. With regards to this, a rapid, label-free, low-cost, and sensitive diagnostic tool is quite in demand for CEA detection.

In view of the limitations of CLIA and ELISA, label-free biosensing by plasmonics shows promising potential for detecting CEA levels [9, 10]. So far, commercial plasmonic

sensor technology has been established on the basis of a prism configuration [11], but it is still cumbersome, inflexible, and uneconomic in the age of Internet of things [12]. Therefore, in view of future commercialization, exploiting a low-cost portable sensing system with a simple, reliable, and highly sensitive scheme is still a great challenge in the plasmonic biosensing community [13]. In the past few years, nanostructured plasmonic refractive index sensors have attracted a surge of research interest and provided a promising alternative to the prism-based sensors [14–18]. Very recently, Cho's group has also given the systematic review of nanostructured plasmonic sensors for biosensing [19, 20]. They are promising for sufficient sensitivity with significantly reduced detection spot size and facilitate device miniaturization and parallel detection of multiple species [21, 22]. Many efforts have been made to improve their performance by changing the shape, size, and spatial arrangement of plasmonic nanostructures [23–26]. Despite of the long-term efforts, there are still no products available in the market of tumor marker examination on the basis of these nanostructured plasmonic sensors, because of the lack of reliability, stability, practical portability, and low expense. In the previous work, we have illuminated that the plasmonic nanocave array (PNA) based on a reflection measurement possesses excellent bulk refractive index sensitivity with a simple configuration and has the capability to approach an ultra-high figure of merit [27, 28]. The inexpensive production and operation based on the ultra-sensitive PNA substrates have also been developed, which indicates that the PNA sensors are promising candidates for portable detection of CEA. However, only the implementation of high-performance PNA sensors still deviates common clinical tests of CEA with the requirement of high throughput for multi-individuals or multi-makers. In practice, it is beneficial to integrate the PNA sensors into standardized functional biochips for clinical applications [29]. Hence, the low-cost mass production of uniform PNA, the functionality of fabricated plasmonic nanostructures, the multichannel sensing on a microfluidic chip, the simplicity of detection configuration, and the reliability and compatibility with authentic serum samples are all significant issues for developing a portable biosensing system for applications on mobile healthcare. Up to now, the entirety of these issues has not been systematically investigated yet.

Here, we use a low-cost scheme for portable rapid detection of CEA with high sensitivity, as shown in Figure 1A. The biosensing chips are fabricated by a cost-effective method in combination with high-sensitivity PNA sensors and multichannel microfluidics, as shown in Figure 1B. We adopt a convenient and low-cost fiber probe for the measurement. These chips are proved to have a

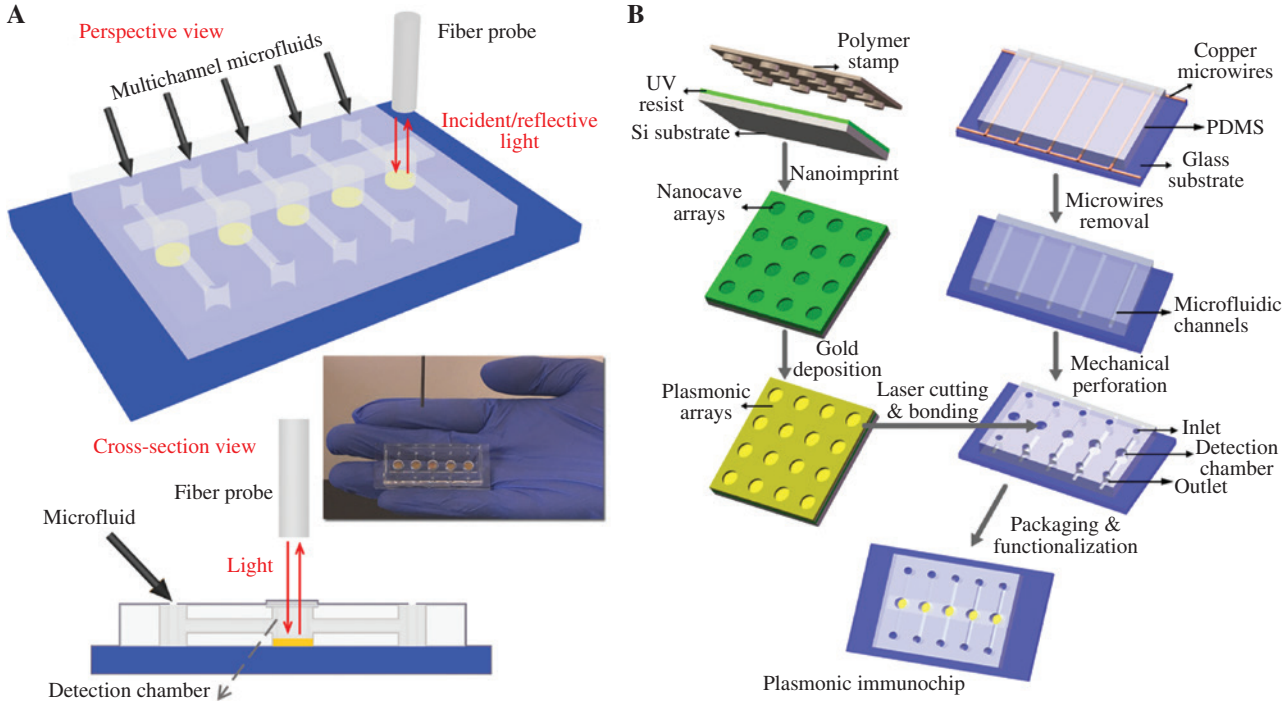

Figure 1: Sensing configuration and biochip fabrication.
(A) Schematic drawing of a plasmonic immunochip with a fiber probe. Inset is a photo of the immunochip and fiber probe. (B) Schematic drawing of the fabrication process of the plasmonic immunochip.

quick response within 30 min and an effective detecting sensitivity in applications and imply promising potentials for point-of-care diagnosis and mobile healthcare.

2 Experimental

2.1 Materials and characterization methods

Soft transparent polymer stamps and TU-170 UV nanoimprint resist are from Obducat AB (Lund, Sweden). 1-Ethyl-3-(3-dimethylaminopropyl)carbodiimide hydrochloride (EDC), *N*-hydroxysuccinimide (NHS), and phosphate buffer saline (PBS) are from LvYin Reagent (Xiamen, China). Polydimethylsiloxane (PDMS) is from Dow Corning (Midland, MI, USA). 11-Mercaptoundecanoic acid (MUA) is from Cool Chemistry (Beijing, China). Bovine serum albumin (BSA) is from Sangon Biotech (Shanghai, China). CEA, anti-CEA, α-fetoprotein (AFP), ferritin (Fer), carbohydrate antigen 19-9 (CA 19-9), and anti-CA 19-9 are from Siemens Healthcare Diagnostics (New York, NY, USA). The carbohydrate antigen 242 (CA 242) and anti-CA 242 are from Shenzhen New Industries Biomedical Engineering (Shenzhen, China). Scanning electron microscope (SEM; Hitachi S-4800) and atomic force microscopy (AFM; SPA400) systems are used to characterize the morphology of PNA surface.

In order to authenticate the changes on gold surface by functionalization of nanoimprinted chips, electrochemical measurements are performed by a CHI660 electrochemical workstation from CH Instruments (Austin, TX, USA) with a three-electrode system, which includes an auxiliary platinum electrode, a reference saturated calomel electrode, and a gold electrode as the working electrode. We have carried out measurements for the gold electrode surface without functionalization, with MUA, and with MUA/anti-CEA, respectively. For each measurement, the gold electrode is washed by deionized water thoroughly and immersed in a solution of 5 mM potassium ferricyanide. Voltammetry measurements have been performed for a potential range from −0.2 to 0.7 V at a sweep rate of 0.1 V/s.

2.2 Fabrication of immunochips

As shown in Figure 1B, in the soft nanoimprint process, a polymer stamp is used to duplicate the nanocave arrays on a 2 in nickel mold by thermal nanoimprint, and a 2-inch silicon wafer spin-coated by the UV resist of about 210 nm is covered by the polymer stamp and processed at 65°C with a pressure of 30 bar for 1 min. After UV exposure, the wafer is etched by oxygen plasma and evaporated by 5 nm chromium and 250 nm gold. The PNA wafer is cut into small pieces (5 mm in diameter) by a laser cutting machine in order to be integrated with the microfluidic chip.

In the fabrication process of microfluidic channels shown in Figure 1B, copper microwires with a diameter of 150 μm are fixed on a rectangle mold, and PDMS is then cast on the mold and kept at 60°C for 3 h. After that, the PDMS is dip in ethanol for 10 min, and the microwires are pulled out. Next, the PDMS is heated in an oven at 60°C for 30 min, and microfluidic inlets, outlets, and detection chambers are perforated by a mechanical mold. A glass substrate, PNA pieces, and a glass cover slice are sequentially bonded and integrated into an entire packaged chip. Redundant openings of microfluidic channels are treated and blocked by a small quantity of unsolidified PDMS at 60°C for 3 h.

The PNA pieces in the detection chambers are antibody-functionalized by covalently immobilizing anti-CEA (or anti-CA 19-9/anti-CA 242) onto the thiolated modified surfaces of PNA, as shown in Figure 2. In this process, 1 mM MUA solution of ethanol is injected into the detection chambers through the inlets of microfluidic channels and maintained for 3 h to form a self-assembled monolayer on the surface of PNA. After that, the MUA solution is exhausted from the chip, and ethanol and deionized water are injected into the microfluidic channels and chambers for thorough cleaning. Next, a solution with 400 mM EDC and 100 mM NHS is injected into the detection chambers and maintained for 30 min in order to activate the MUA monolayer, which is followed by extracting the solution and cleaning with deionized water. Finally, 40 μg/ml of anti-CEA (or anti-CA 19-9/anti-CA 242) solution is injected and maintained for 1 h in order to immobilize the antibody on the PNA surface, BSA (1 wt%) is injected to block the remaining activated carboxylic groups and to prevent nonspecific adsorption from human serums on the sensing surface, and the chip is injected and washed with deionized water and ready for use. In order to ensure the consistency of experiments, all the solutions injected to the chambers are overflowing each time.

2.3 Optical measurement and simulation

A reflection optical fiber probe in combination with a portable UV-visible spectrometer from Avantes BV (Apeldoom, Netherlands) is used to measure the optical spectra of all the PNA surfaces in the detection chambers. The fiber

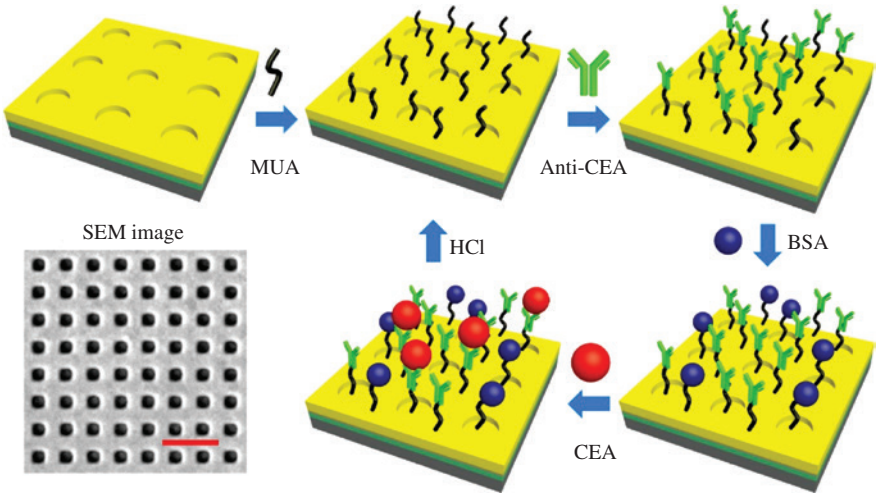

Figure 2: Schematic drawing of functionalization, detection, and recycling for the PNA surface.
The SEM image of the PNA surface is provided in the left corner, with the red scale bar of 1 μm. (The schematic drawing does not represent the precise sizes of the adsorbed materials compared with the dimensions of nanocaves.)

probe consists of six lighting fibers and one reading fiber (200 μm core) with an operational range in the visible region. In optical measurements, the fiber probe is perpendicularly located on top of the chamber with a distance of ~2 mm to the glass cover of the chip, and the reflectance from a silver mirror is used as a spectral reference. At each measurement, the detection chamber is washed thoroughly and filled with deionized water. A full-wave finite element numerical method is used to simulate the optical reflectance of PNA under normal incidence by adopting infinite unit cells with Floquet periodic boundary conditions. We simply assume that the gold nanocaves have a circular shape for a theoretical approximation. The optical constants of gold are obtained from the literature [30]. Adaptive inhomogeneous tetrahedral mesh is adopted to discretize the unit cell, and the minimum edge length of the mesh element is as small as 0.5 nm to ensure the convergence and reproducibility of numerical simulations [31].

2.4 Detection of CEA

The detection of CEA is based on its specific binding on the anti-CEA (40 μg/ml in PBS). In order to indicate the specificity of CEA for the immunochip, five kinds of PBS solutions of 20 ng/ml CEA, 30 ng/ml AFP, 100 ng/ml Fer, 20 ng/ml CEA in combination with 30 ng/ml AFP, and 20 ng/ml CEA in combination with 100 ng/ml Fer are injected into five separate microfluidic chambers, respectively. The chambers are filled with the solutions for 30 min and followed by the optical measurements with the reflection optical probe. Five groups of CEA solutions with various concentrations of 5, 10, 20, 30, and 40 ng/ml are injected into five separate chambers, incubated for 30 min, and followed by the optical measurements with the reflection fiber probe. For each CEA concentration, we adopt three groups of solution for spectral measurements, which are further used for s.d. calculations. The chips used for antigen detection can be recycled by removing proteins adsorbed on the PNA surface. As shown in Figure 2, after the antigen detection, 0.5 mol/l hydrochloric acid solution is injected into the chambers, maintained for 20 min, and washed thoroughly by deionized water. Spectral measurements are performed to verify the result of the recycling process.

2.5 Diagnosis of tumor markers in human serums

All the human serum samples are collected by the First Affiliated Hospital of Xiamen University (Xiamen, China) with the consent from some individuals and are analyzed in advance by ADVIA Centaur XP Immunoassay System (Erlangen, Germany), which is based on CLIA. The serum samples are stored at –20°C and used for the immunochip diagnosis at room temperature after thawing. Six serum samples from different individuals are injected into their respective detection chambers through microfluidic channels on the chip and allowed for the immunological reaction of CEA for 30 min. After that, the serums are extracted, and the detection chambers filled with deionized water are measured by the reflection optical probe. The concentration of CEA is determined on the basis of

the optical sensing curve obtained in Section 2.4. Additionally, a serum sample from one individual is injected into three separate microfluidic chambers immobilized by anti-CEA, anti-CA 19-9, and anti-CA 242, respectively. After incubating for no more than 30 min, multiple tumor markers from the same serum is detected simultaneously in the immunochip.

3 Results and discussion

3.1 Analysis of plasmonic nanostructures

The 2 in PNA wafers are fabricated by soft UV nanoimprint and gold deposition [32]. The plasmonic sensing components integrated in the detection chambers are cut out from the PNA wafers. The soft UV nanoimprint is a versatile and inexpensive fabrication method for mass production of nanostructures [33, 34]. As shown in the SEM image of Figure 2, the gold nanocaves are uniform with the periodic spacing of ~500 nm and the diameter of ~250 nm, and the depth of ~200 nm for the nanocaves is also confirmed by an AFM system (Figure S1). The structure uniformity in a large area benefits the specification of standard and unified PNA sensors for plasmonic immunochips. The gold nanocaves act as two-dimensional arrays with orthogonal reciprocal lattice vectors, which allows for the grating-coupled plasmon modes and traps the spatial light around the resonant wavelength. The resonant wavelengths of these modes under normal incidence can be estimated by the following equation [35, 36]:

$$\lambda = \frac{P}{\sqrt{m^2 + n^2}} \sqrt{\varepsilon \varepsilon_{Au} / (\varepsilon + \varepsilon_{Au})} \quad (1)$$

where P, integers (m, n), ε_{Au}, and ε represent the periodicity of gold nanocaves, the order of plasmonic mode, the permittivity of gold, and the environmental permittivity surrounding the gold surface, respectively. On the basis of equation (1), the period around 500 nm is selected by considering the plasmonic light confinement in the visible range (especially for the sensing in the solution), which facilitates the use of the low-cost photodetector of visible light. The diameter of 250 nm and the depth of 200 nm are large enough to contain and adsorb MUA, antibodies, and antigens, which might have dimensions of up to tens of nanometers. The selection for the geometry, dimensions, and periodicity of the PNA are also determined by the related references [15, 19]. As shown in the reflectance spectrum of Figure 3A, the resonant wavelength of the (1,

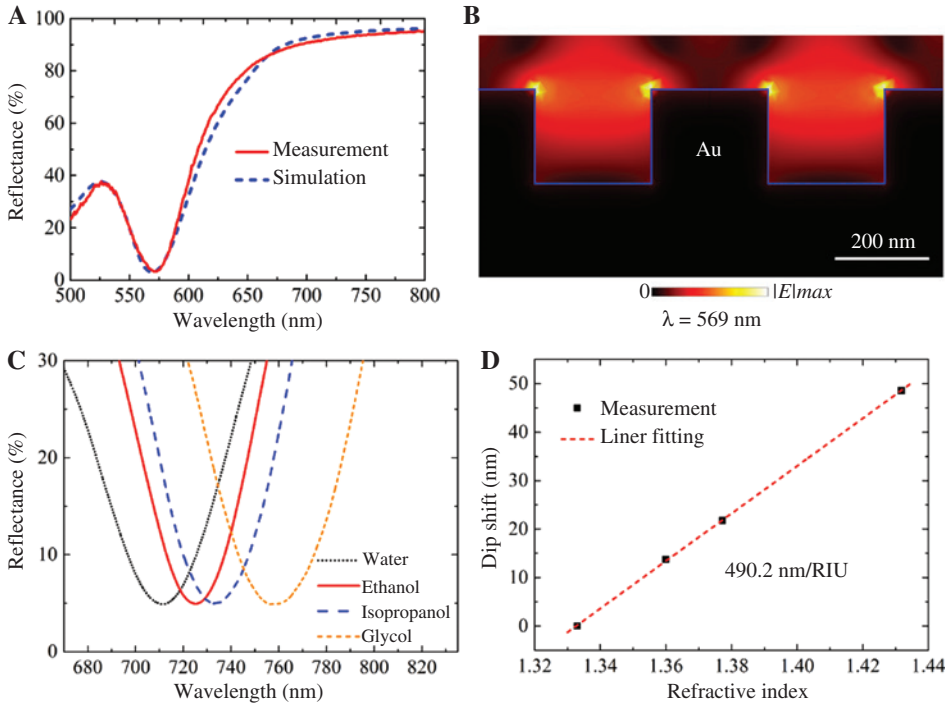

Figure 3: Optical performance of PNA.
(A) Measured and simulated reflectance spectra of bare PNA under normal incidence in the air. (B) Electric field distribution for the (1, 0) order plasmonic resonance mode at $\lambda = 569$ nm. (C) Reflectance spectra of the (1, 0) order resonance in the PNA for various solvents. (D) Reflectance dip shift of the (1, 0) order resonance as a function of refractive index.

0) order plasmonic mode is indicated by the spectral dip around $\lambda = 569$ nm, which is due to the light confinement and resonant dissipation in gold under normal incidence from the air. Figure 3A also demonstrates that the optical simulation has good consistency with the spectral measurement, which further confirms our theoretical analysis. The electric field distribution of the resonant mode is illustrated in Figure 3B, and it indicates that the electric fields are tightly confined and enhanced surrounding the periodic nanocaves, which enables the sensitive detection of materials captured on the PNA surface. The estimated electromagnetic field decay length on top of the PNA surface is within the scale of around 100 nm. On this condition, the length scale of the detected protein molecules in our experiments would remain within the enhanced electromagnetic field decay length. Such a decay length is larger than that of biosensors based on localized surface plasmon resonance (10–30 nm) and smaller than that of conventional biosensors based on surface plasmon resonance (hundreds of nanometers) [19]. This scale design is well fit for the accumulated lengths of MUA, antibodies, and antigens in our detection.

In order to evaluate the detection sensitivity of the PNA surface, bulk refractive index measurements are performed by successively immersing the same PNA sensor in four different solvents, including deionized water, ethanol, isopropanol, and glycol. As shown in Figure 3C, the reflectance dip of the (1, 0) order resonance shifts to longer wavelengths because of the increase of the refractive index (or permittivity) surrounding the gold nanocaves, which is consistent with the estimation by equation (1). The shift of the resonant dip as a function of refractive index is plotted in Figure 3D, and the error bars of measured data are too small to be observed. Figure 3D shows that the sensitivity of bulk refractive index is as high as 490.2 nm/RIU in the visible range, which is advantageous and sufficient for high-sensitivity biosensing compared with other plasmonic surfaces by nanoimprint lithography [37, 38]. In view of the adsorbed materials, including MUA, anti-CEA, and CEA, their sizes are much smaller than the diameter of nanocaves (~250 nm), and they can be equally adsorbed on the top surface and the interior of the nanocaves. On the basis of equation (1), ε can also be considered as an effective permittivity combining the adsorbed materials and the surrounding solvent, and the resonant wavelength increases as the effective permittivity (or effective refractive index) becomes larger. Specific binding of CEA with various concentrations to the PNA sensing surface changes the local refractive index differently, which can be monitored by measuring wavelength shifts of the resonant dip. This fundamental physics provides a convincing guide for the study of plasmonic sensors on the basis of gold nanocaves.

In addition, the use of gold nanocave array has several advantages in view of practical applications. First, the entire sensing surface is encapsulated by gold, and this benefits the process of antibody functionalization, in which the superficial gold needs to be thiolated by MUA in advance. Second, gold is chemically stable, and only the material exposure of gold will maintain the steadiness of the plasmonic sensors, especially for the recycling procedure by treatment of HCl. Third, instead of plasmonic angular coupling on a prism or transmission measurement by a microscope, the PNA allows the reflection scheme of normal incidence with the illumination source and the photodetector at the same side, which facilitates the integration for a compact portable detection system. Fourth, the operational wavelengths of the nanostructure are controlled within the visible range, which enables the use of low-cost charge-coupled digital camera devices for portable applications.

3.2 Immobilization of PNA with anti-CEA

Sufficient immobilization of active antibody on the gold surface is a critical procedure for biomarker detection based on plasmonics [39, 40]. In our study, a self-assembled monolayer of MUA is adopted as an intermediate material layer to immobilize anti-CEA on the gold surface by the scheme of covalent-bonding. In order to confirm that MUA and anti-CEA are immobilized on the surface of PNAs, optical reflectance measurements and electrochemical measurements are performed for further analysis, as shown in Figure 4A and B. As observed in Figure 4A, compared with the spectrum of PNA without immobilization, the spectra redshifted to 3.46 and 7.47 nm for the PNA with MUA and the PNA with MUA/anti-CEA, respectively, because of the increase of local refractive index. The spectral characterization for the sensing surface in the air is also performed by nitrogen drying and reflectance measurements after each immobilization step (Figure S2), and the resonant dip shift further illuminates the steady bonding of MUA and anti-CEA on the PNA surface.

The antibody functionalization is also evaluated by electrochemical measurements using a gold electrode, as shown in Figure 4B. The voltammetric curve for each immobilization step implies the conductive behavior of the gold electrode surface, and $[Fe(CN)_6]^{3-}$ ions in the solution act as an electrochemical probe for

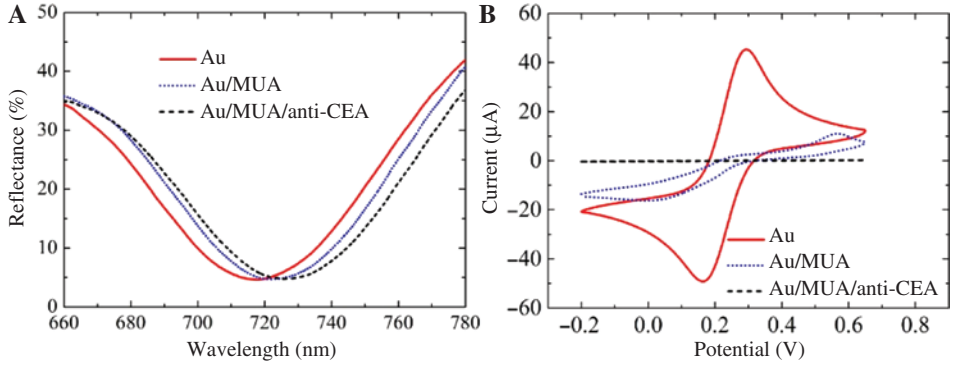

Figure 4: Characterizations of bare gold, gold with MUA, and gold with MUA/anti-CEA.
(A) Reflectance spectra with filled deionized water in detection chambers. (B) Electrochemical voltammetry measurement of a gold electrode.

the surface change. The peak current due to the redox process decreases significantly when MUA is immobilized on the gold surface, because the long chain MUA has no conductivity and its negative charge obstructed $[Fe(CN)_6]^{3-}$ ions diffusing to the gold electrode surface. As anti-CEA is bound on Au/MUA, the electrode surface tends to electro-neutrality, and there is no obvious current peak observed. On the basis of the above results, both the measurements of optical spectra and electrochemical voltammetry demonstrate that MUA and anti-CEA are immobilized on the PNA surface subsequently as anticipated.

3.3 Immunologic specificity

The developed plasmonic immunochips are intended for ultimate CEA detection in human serums. As the composition of human serum is complex, including a variety of antibodies and antigens, the anti-CEA functionalized on the surface of PNA should have the capability to capture CEA only for diagnosis detection. In order to confirm this, the solutions of AFP (~70 kDa), CEA (~200 kDa), and Fer (~474 kDa) are applied to test the selectivity of the immunochip for CEA detection. These three antigens have various molecular sizes, which are much smaller than the diameter and depth of the nanocaves, and they can be contained on the top surface of the array and in the interior of nanocaves when the solutions are applied on the plasmonic sensor to test the immunologic specificity of anti-CEA. As shown in Figure 5A, there is no shift of resonance wavelength for the solutions of 100 ng/ml Fer and 30 ng/ml AFP, whereas there is the same red shift of ~2.3 nm for the other three solutions with the same CEA concentration of 20 ng/ml. This is because the surface of functionalized PNA only captured CEA specifically from the solutions without CEA, and there is no specific binding of Fer or AFP on the surface. Additional

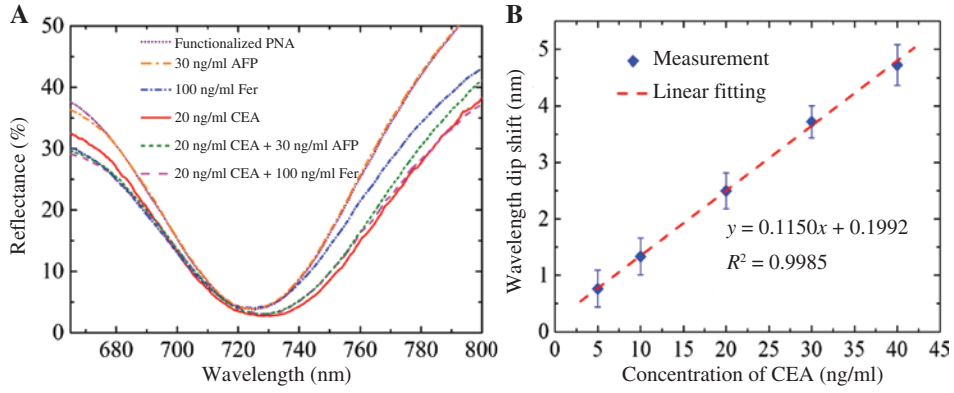

Figure 5: Immunologic specificity and sensing capability.
(A) Reflectance spectra of specific tests. (B) Resonant wavelength dip shift as a function of CEA concentration. The fitting line is based on measurements from 5 to 40 ng/ml, and the error bars are based on s.d. calculation for three data points measured at each concentration. The linear fitting function *y* and correlation coefficient *R* are denoted in the plot.

evidences by AFM and energy dispersive spectrometer are also provided in Figures S3 and S4 to confirm the capture of CEA. These results indicate the immunologic specificity of our chips for CEA detection.

In view of waste recycling and environmental protection, we have recycled used plasmonic immunochips. The 0.5 mol/l hydrochloric acid solution is injected to treat the surface of PNA immobilized with the antibody and antigen, and the performance for five runs of recycling is verified by comparing its optical spectra before and after the treatment. As observed in Figure S5, the wavelength of plasmonic resonance after the acid treatment is the same as that of the original plasmonic surface with MUA, which demonstrates the reproducibility and stability of recycled chips for CEA detection.

3.4 Sensing capability of immunochips

In order to test the sensitivity of plasmonic immunochips, we incubate five detection chambers with different concentrations of CEA ranging from 5 to 40 ng/ml. The largest detected concentration of 40 ng/ml is controlled within the range of antigen saturation on the PNA surface. All measurements have the same incubation time and the same liquid volume in the microfluidic channels and detection chambers, with the aim of ensuring the measurement precision. On the basis of the measured spectra (Figure S6), the concentration-dependent shift of plasmonic resonant dip is summarized in Figure 5B, in which the dip shift increased proportionally to the CEA concentration. The linear fitting has a correlation coefficient R of 0.9985, which is very close to the value 1 and demonstrates very good linear relationship between concentration of CEA and resonant wavelength dip shift. In our system, the detection of 5 ng/ml CEA solvent can be clearly designated in experiments, which is much lower than the threshold concentration of 20 ng/ml for early cancer prediction. It is worth mentioning that, in all the measurements, the microfluidic channels and detection chambers are filled with corresponding operational solvents. This not only keeps the activity of adsorbed anti-CEA and CEA in detection but also avoids inconvenient drying of the PNA in the microfluidic chips. Additionally, the detection with filled solvents is more versatile for the application of microfluidic chips and ensures quantitative analysis and detection precision. Therefore, the plasmonic biochips functionalized by anti-CEA provide an exceptional sensing capability for label-free, convenient, sensitive, and reliable detection of CEA.

3.5 Rapid detection of human serums with microfluidic channels

The performance of quantitative CEA detection by the chip for medicine has been validated by testing the serum samples from six individuals, and the results are compared with measurements from CLIA in The First Affiliated Hospital of Xiamen University (Xiamen, China). As shown in Figure 6A, the results detected by the plasmonic immunochips demonstrate good agreement with the results from CLIA. When the detected concentration of CEA in serum is higher than 10 ng/ml, there is a deviation of less than |±5.9%| in comparison with the conventional clinical examination. The chip detections for six individuals have been performed concurrently and completed in 30 min in room temperature (Figure S7), which demonstrates the potential advantage of combining nanoimprint and microfluidics for high-throughput quantitative analysis of CEA. On the basis of the tested results from Serum 1 to Serum

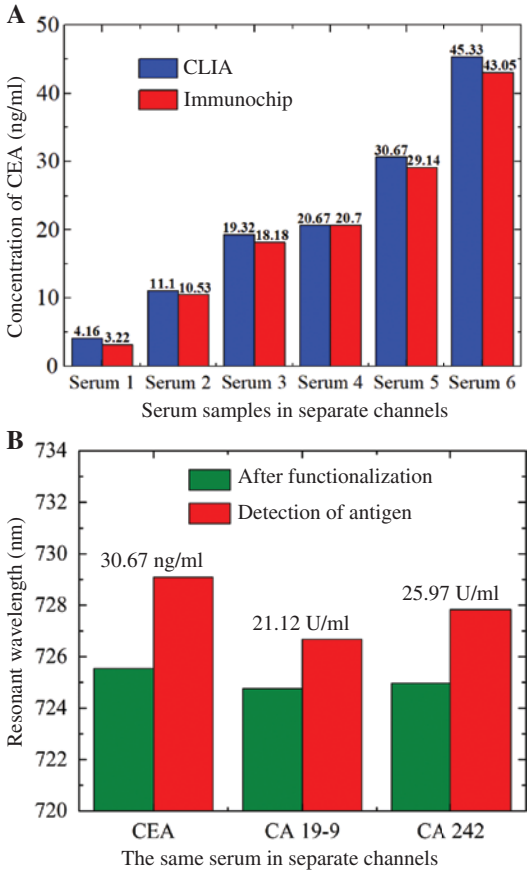

Figure 6: Detection of human serums.
(A) CEA detection results of serum samples from six individuals using the plasmonic immunochip, compared with using CLIA.
(B) Concurrent sensing of three tumor markers in separate microfluidic channels.

6 in Figure 6A, Individual 1, Individual 2, and Individual 3 have a CEA concentration lower than 20 ng/ml, which is a normal level and might imply the healthy status; the CEA concentrations for Individual 4, Individual 5, and Individual 6 are higher than the threshold of 20 ng/ml, which might indicate the disease of tumor.

Besides, the clinical detection of CEA for tumor diagnosis has been adopted for many years, but only CEA detection might be incomplete for accurate prognosis of the type of tumor. A type of tumor usually caused higher levels of many kinds of biomarker in the serum [41]. For instance, the combined detections of CEA, CA 19-9, and CA 242 provide significant evidences for the precise diagnosis and prognosis of pancreatic carcinoma [42]. In view of the detection importance of multi-tumor markers, we have performed a proof-of-concept experiment for the simultaneous sensing of CEA, CA 19-9, and CA 242 in the serum of one individual. As shown in Figure 6B, by using three separated microfluidic channels, the three kinds of tumor markers are sensed by the shift of plasmonic resonant wavelength within 30 min. This implies the promising potential of the chips for comprehensive and accurate detection of various kinds of cancer.

4 Conclusions

In summary, we have introduced nanoimprinted plasmonic immunochips with microfluidics for rapid and sensitive detection of CEA in human serums. The immunochips are prepared through functionalizing the PNA surface with anti-CEA and used to specific, quantitative, and label-free detection of CEA. The plasmonic design provides exceptional sensitivity and allowed for the simple measuring configuration. By the measurements in multiple microfluidic channels, the detection capability for the CEA concentration below and above the threshold of 20 ng/ml is effectively achieved, and the parallel detection time for many individuals and the multi-biomarker sensing for one individual are both controlled within 30 min. Compared with conventional detection techniques, our method is not only cost-effective and label-free but also high-throughput and comprehensive for precise cancer diagnosis and prognosis. The plasmonic immunochip based on low-cost manufacture and compact configuration will have a promising future for portable medical devices/systems in point-of-care diagnosis and mobile healthcare.

Acknowledgments: This work was supported by NSAF (grant no. U1830116), China Scholarship Council, Fujian Provincial Department of Science and Technology (grant no. 2017J01123), NSFC (grant no. 61307042), and University of Southampton Zepler Institute Research Collaboration Stimulus Fund (517719105) enabled by the 2017/18 UK Higher Education Innovation Fund.

References

[1] Wada N, Kurokawa Y, Miyazaki Y, et al. The characteristics of the serum carcinoembryonic antigen and carbohydrate antigen 19-9 levels in gastric cancer cases. Surg Today 2017;47:227–32.
[2] Duffy MJ, Lamerz R, Haglund C, et al. Tumor markers in colorectal cancer, gastric cancer and gastrointestinal stromal cancers: European group on tumor markers 2014 guidelines update. Int J Cancer 2014;134:2513–22.
[3] Shimada H, Noie T, Ohashi M, Oba K, Takahashi Y. Clinical significance of serum tumor markers for gastric cancer: a systematic review of literature by the Task Force of the Japanese Gastric Cancer Association. Gastric Cancer 2014;17:26–33.
[4] Metildi CA, Kaushal S, Pu M, et al. Fluorescence-guided surgery with a fluorophore-conjugated antibody to carcinoembryonic antigen (CEA), that highlights the tumor, improves surgical resection and increases survival in orthotopic mouse models of human pancreatic cancer. Ann Surg Oncol 2014;21:1405–11.
[5] Grunnet M, Sorensen JB. Carcinoembryonic antigen (CEA) as tumor marker in lung cancer. Lung Cancer 2012;76:138–43.
[6] Ebeling FG, Stieber P, Untch M, et al. Serum CEA and CA 15-3 as prognostic factors in primary breast cancer. Br J Cancer 2002;86:1217–22.
[7] Yurkovetsky Z, Skates S, Lomakin A, et al. Development of a multimarker assay for early detection of ovarian cancer. J Clin Oncol 2010;28:2159–66.
[8] van Huijgevoort NC, Hoogenboom SA, Lekkerkerker SJ, et al. The diagnostic accuracy of carcinoembryonic antigen in differentiating mucinous and non-mucinous pancreatic cystic neoplasms – a systematic review and individual patient data meta-analysis. Endoscopy 2018;50:S110–1.
[9] Altintas Z, Uludag Y, Gurbuz Y, Tothilla IE. Surface plasmon resonance based immunosensor for the detection of the cancer biomarker carcinoembryonic antigen. Talanta 2011;86:377–83.
[10] Brolo AG. Plasmonics for future biosensors. Nat Photonics 2012;6:709–13.
[11] Homola J. Present and future of surface plasmon resonance biosensors. Anal Bioanal Chem 2003;377:528–39.
[12] Vashist SK, Luppa PB, Yeo LY, Ozcan A, Luong JH. Emerging technologies for next-generation point-of-care testing. Trends Biotechnol 2015;33:692–705.
[13] Singh P. SPR biosensors: historical perspectives and current challenges. Sens Actuators B Chem 2016;229:110–30.
[14] Shen Y, Zhou J, Liu T, et al. Plasmonic gold mushroom arrays with refractive index sensing figures of merit approaching the theoretical limit. Nat Commun 2013;4:2381.
[15] Im H, Shao H, Park YI, et al. Label-free detection and molecular profiling of exosomes with a nano-plasmonic sensor. Nat Biotechnol 2014;32:490–5.
[16] Hackett LP, Ameen A, Li W, Dar FK, Goddard LL, Liu GL. Spectrometer-free plasmonic biosensing with metal-insulator-metal nanocup arrays. ACS Sensors 2018;3:290–8.

[17] Li W, Jiang X, Xue J, Zhou Z, Zhou J. Antibody modified gold nano-mushroom arrays for rapid detection of alpha-fetoprotein. Biosens Bioelectron 2015;68:468–74.
[18] Le T, Tanaka T. Plasmonics-nanofluidics hydrid metamaterial: an ultrasensitive platform for infrared absorption spectroscopy and quantitative measurement of molecules. ACS Nano 2017;11:9780–8.
[19] Jackman JA, Ferhan AR, Cho NJ. Nanoplasmonic sensors for biointerfacial science. Chem Soc Rev 2017;46:3615–60.
[20] Ferhan AR, Jackman JA, Park JH, Cho NJ, Kim DH. Nanoplasmonic sensors for detecting circulating cancer biomarkers. Adv Drug Deliver Rev 2018;125:48–77.
[21] Špačková B, Wrobel P, Bocková M, Homola J. Optical biosensors based on plasmonic nanostructures: a review. P IEEE 2016;104:2380–408.
[22] Lopez GA, Estevez MC, Soler M, Lechuga LM. Recent advances in nanoplasmonic biosensors: applications and lab-on-a-chip integration. Nanophotonics 2017;6:123–36.
[23] Cetin AE, Etezadi D, Galarreta BC, Busson MP, Eksioglu Y, Altug H. Plasmonic nanohole arrays on a robust hybrid substrate for highly sensitive label-free biosensing. ACS Photonics 2015;2:1167–74.
[24] Aćimović SS, Ortega MA, Sanz V, et al. LSPR chip for parallel, rapid, and sensitive detection of cancer markers in serum. Nano Lett 2014;14:2636–41.
[25] Sreekanth KV, Alapan Y, Elkabbash M, et al. Extreme sensitivity biosensing platform based on hyperbolic metamaterials. Nat Mater 2016;15:621–7.
[26] Li W, Zhang L, Zhou J, Wu H. Well-designed metal nanostructured arrays for label-free plasmonic biosensing. J Mater Chem C 2015;3:6479–92.
[27] Liu B, Chen S, Zhang J, et al. A plasmonic sensor array with ultrahigh figures of merit and resonance linewidths down to 3 nm. Adv Mater 2018;30:1706031.
[28] Zhu J, Bai Y, Zhang L, et al. Large-scale uniform silver nanocave array for visible light refractive index sensing using soft UV nanoimprint. IEEE Photonics J 2016;8:6804107.
[29] Cetin AE, Coskun AF, Galarreta BC, et al. Handheld high-throughput plasmonic biosensor using computational on-chip imaging. Light Sci Appl 2014;3:e122.
[30] Palik ED. Handbook of optical constants of solids. San Diego, CA, USA, Academic Press, 1998.
[31] Zhu J, Yan S, Feng N, Ye L, Ou JY, Liu QH. Near unity ultraviolet absorption in graphene without patterning. Appl Phys Lett 2018;112:153106.
[32] Zhu J, Zhang L, Bai Y, et al. Simultaneous fabrication of two kinds of plasmonic crystals by one nanoimprint mold. IEEE Photonic Tech L 2017;29:504–6.
[33] Cattoni A, Ghenuche P, Haghiri-Gosnet AM. λ^3/1000 plasmonic nanocavities for biosensing fabricated by soft UV nanoimprint lithography. Nano Lett 2011;11:3557–63.
[34] Leitgeb M, Nees D, Ruttloff S, et al. Multilength scale patterning of functional layers by roll-to-roll ultraviolet-light-assisted nanoimprint lithography. ACS Nano 2016;10:4926–41.
[35] Ghaemi HF, Thio T, Grupp DE, Ebbesen TW, Lezec HJ. Surface plasmons enhance optical transmission through subwavelength holes. Phys Rev B 1998;58:6779–82.
[36] Van der Molen KL, Segerink FB, Van Hulst NF, Kuipers L. Influence of hole size on the extraordinary transmission through subwavelength hole arrays. Appl Phys Lett 2004;85:4316–8.
[37] Yang SC, Hou JL, Finn A, Kumar A, Ge Y, Fischer WJ. Synthesis of multifunctional plasmonic nanopillar array using soft thermal nanoimprint lithography for highly sensitive refractive index sensing. Nanoscale 2015;7:5760–6.
[38] Escobedo C. On-chip nanohole array based sensing: a review. Lab Chip 2013;13:2445–63.
[39] Wijaya E, Lenaerts C, Maricot S, et al. Surface plasmon resonance-based biosensors: From the development of different SPR structures to novel surface functionalization strategies. Curr Opin Solid State Mater Sci 2011;15:208–24.
[40] Beuwer MA, Prins MW, Zijlstra P. Stochastic protein interactions monitored by hundreds of single-molecule plasmonic biosensors. Nano Lett 2015;15:3507–11.
[41] Wu J, Fu Z, Yan F, Ju H. Biomedical and clinical applications of immunoassays and immunosensors for tumor markers. Trends Anal Chem 2007;26:679–88.
[42] Ni XG, Bai XF, Mao YL, et al. The clinical value of serum CEA, CA19-9, and CA242 in the diagnosis and prognosis of pancreatic cancer. Eur J Surg Oncol 2005;31:164–9.

Supplementary Material: The online version of this article offers supplementary material (https://doi.org/10.1515/nanoph-2018-0173).